International Conference on Space Optics—ICSO 2022

Dubrovnik, Croatia

3–7 October 2022

Edited by Kyriaki Minoglou, Nikos Karafolas, and Bruno Cugny,

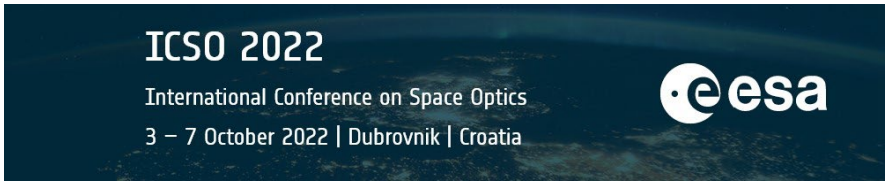

Study of Laser Ablation Induced Impulse for Laser Space Debris Removal

International Conference on Space Optics — ICSO 2022, edited by Kyriaki Minoglou, Nikos Karafolas, Bruno Cugny, Proc. of SPIE Vol. 12777, 1277762 · © 2023 ESA and CNES · 0277-786X · doi: 10.1117/12.2691109

Study of Laser Ablation Induced Impulse for Laser Space Debris Removal

Katsuhiko Tsuno[a], Satoshi Wada[a], Takayo Ogawa[a], Norihito Saito[a], Tadanori Fukushima[a,b], Toshikazu Ebisuzaki[a], Yusuke Nakamura[c], and Akihiro Sasoh[c]

[a]RIKEN, 2-1 Hirosawa, Wako, Japan
[b]SKY Perfect JSAT, AKASAKA Intercity AIR 11th floor, 1-8-1, Aksaka, Minato-ku, Tokyo, Japan
[c]Nagoya University, Furo-cho, Chikusa-ku, Nagoya, Japan

ABSTRACT

Even a low failure rate means that dozens of satellites could lose control and become debris. Because they are located in an operational orbit, they pose a serious problem. Therefore, a few active debris removal (ADR) ideas have been proposed, which is to tow and de-orbit debris satellites with rescue satellites similar to tugboats for shipwrecks. In these cases, physical contact, such as towing by wire, is a prerequisite. Mechanical coupling between satellites involves risks such as the collision between satellites and loss of attitude control at the time of coupling. Since no cooperation between the two satellites is not desirable, mechanical contact is very difficult when the debris has high angular momentum. On the other hand, the contactless debris removing idea, to irradiate debris satellites with lasers and use of the laser ablation induced impulse, has been proposed. In this approach ti, is important to accumulate data on how much impulse is generated by the plasma plume produced by laser ablation in a vacuum. A compact and efficient measurement device to measure this impulse has been developed. In this study, we investigated impulses generated by a 10ns Q-switched Nd:YAG laser (1064nm) and its second harmonic generation (SHG, 532nm) using a metal as a target for laser irradiation. The results show that the fundamental (1064nm) laser of about 100W can generate enough thrust to deorbit space debris with comparable mass to a small satellite from 1000km to 500km altitude in a year. SHG can be converted to impulse more efficiently than 1064nm. The use of 532nm alone, including the SHG generation efficiency, has less impact on the impulse generation effect than the use of 1064nm fundamental alone, without SHG. It was pointed out that the energy of the Nd:YAG laser effectively uses generation of impulse when the remaining fundamental components that could not be converted to SHG could be used to irradiate to generate ablation. Although the use of SHG is not effective in terms of 1064nm fundamental power including SHG generation efficiency, it is demonstrated that the energy of the Nd:YAG laser can be efficiently utilized by using the remaining fundamental components that could not be converted to SHG.

Keywords: Laser Induced Ablation, Laser Induced Impulse, Space Debris, Orbital Debris, Nd:YAG Laser, SHG

1. INTRODUCTION

The laser induced ablation in a vacuum has attracted considerable attention for various space applications, such as the laser induced ablation thruster,[1] laser thrust rocket launcher,[1] and laser-induced breakdown spectroscopy

Further author information: (Send correspondence to K.T.)
K.T.: E-mail: tsuno@riken.jp, Telephone: +81 50 3502 3524
S.W.: E-mail: swada@riken.jp
T.O.: E-mail: pogawa@riken.jp
T.F.: E-mail: t-fukushima@sptvjsat.com
N.S.: E-mail: norihito@riken.jp
T.E.: E-mail: ebis@riken.jp
Y.N.: E-mail: yusuke.nakamura@mae.nagoya-u.ac.jp
A.S.: E-mail: akihiro.sasoh@mae.nagoya-u.ac.jp

(LIBS).[2] A recent large low Earth orbit (LEO) constellation program used several thousand "small satellites", which is a satellite class with a mass of a few hundred kg. Even a low failure rate means that dozens of satellites could lose control and become debris. Because they are located in an operational orbit, they pose a serious problem. Therefore, a few active debris removal (ADR) ideas have been proposed, which is to tow and de-orbit debris satellites with rescue satellites similar to tugboats for shipwrecks[3].[4] In these cases, physical contact, such as towing by wire, is a prerequisite. Mechanical coupling between satellites involves risks such as the collision between satellites and loss of attitude control at the time of coupling. In the rendezvous and docking process, the two satellites usually prepare the docking mechanisms at specific locations and exchange information about attitude and distance with each other. Both satellites control facing each other with docking mechanisms and ensure safe mechanical contact. In the case of debris capture, the attitude and distance of the debris must be identified by remote sensing. The system has not only a docking mechanism, but the satellite is also hard to make mechanical contact with a specific surface of the debris. Mechanical contact is very difficult when the debris has high angular momentum.

A practical system on board the small satellite has been proposed. The system rendezvous with the debris to allow a longer laser irradiation period and require 100W average laser power to deorbit the debris satellite in the order of 100kg.[5]

In this case, any contact between the debris satellite and the rescue satellite is not required. The angular momentum of the debris satellite can also be controlled, when the laser irradiating position on the debris is controlled. In this case, the greater the impulse induced by laser ablation, the more quickly the same satellite mass, and/or large debris satellites can be deorbited within the same period. So it is important to know the efficiency and characteristics of the impulse generated by ablation in a vacuum.

The idea of a contactless method to deorbit debris using the thrust generated by laser ablation has been proposed by Schall[6] in 1991. In this proposal, a laser with an average power of 100 kW is required to remove debris of the order of 10cm in a short encounter time to it. A similar high-power laser is mounted on the ISS and a deorbit system for debris in the 10 cm class was proposed[7] in 2015. These systems would require too large resources such as mass, power, and so on, and are not expected to be realized for space use in the foreseeable future.

For the measurements, a new experimental method based on a simple pendulum was introduced. The system was found to have a resolution of 10^{-7}Ns for ablation events induced by a single laser at a pulse rate of 2 Hz or less. For ablation events at a pulse rate of 10 Hz and above, the system recorded the impulse as an average force. The impulse generated by the Nd:YAG laser irradiating A7075 aluminum alloy was investigated. The impulse was generated at 3J/cm^2, and the momentum coupling factor plateaued to approximately 20μNs/J over a range of 5 to 50 J/cm^2 without producing a plasma shielding effect. This result highlights that it should be feasible to deorbit a 150kg abandoned satellite at an altitude of 1000km using a chaser satellite equipped with a 100W laser.[8] The orbit change of the spacecraft is characterized by the velocity change, the so-called "Delta V", $\Delta V = m_s/p_t$, where m_s and p_t are the mass of the spacecraft and total impulse, respectively. Efficient impulse generation means that the heavier space debris will be cleaned in a shorter period, or that the system will be appropriate for smaller spacecraft. The momentum coupling factor C_m is the ratio of the propulsive impulse to the irradiation laser power. The larger the momentum coupling factor, the more efficiently debris can be removed with the same laser power. The generation and heating process of ablation plasma depends on the pulse width through the range from femtoseconds, picoseconds, and nanoseconds, and it is expected to have a significant impact on the coupling coefficient. However, the first high power Q-SW Nd:YAG space laser was demonstrated by Lidar In-Space Technology Experiment (LITE) on board Space shuttle STS-65,[9] and several spaceborne laser missions including planetary exploration missions, for example, Mars Orbiter Laser Altimeter (MOLA)[10] and Lunar Orbiter Laser Altimeter (LOLA),[11] followed. Except for Advanced Topographic Laser Altimeter System (ATLAS)[12] which employed a pulsed fiber laser on board ICESat2, most space missions utilize Q-SW Nd:YAG lasers. In particular, the space lidar systems for atmospheric observation such as Cloud-Aerosol Lidar and Infrared Pathfinder Satellite Observation (CALIPSO),[13] Atmospheric Laser Doppler Instrument (ALADIN),[14] and Atmospheric Lidar (ATLID)[15] use not only the fundamental wave of the Nd:YAG laser but also second harmonic generation (SHG) and third harmonic generation (THG), which

can be generated using nonlinear crystals. Based on the above current status of space lasers, we evaluated the characteristics of Nd:YAG fundamental and SHG. The rest of this paper is structured as follows.

2. MEASURING INSTRUMENTS

2.1 Impulse Stand

A pendulum with a 10 g bob suspended from a 100 mm wire will have a natural frequency $f_0 = \frac{1}{2\pi}\sqrt{g/l}$ of 1.6 Hz and response amplitude of approximately 0.3μm for a 10^{-7}Ns impulse. Fig.1(a) illustrates the impulse measurement stand (IMS) based on the concept of this pendulum system. The four suspension wires restrict the motion of the pendulum mass (PM) to one degree of freedom. A small ablation target is mounted on one side of the PM, while the displacement can be measured on the opposite side. Any contactless displacement sensor, either optical or electrical, with a resolution better than 0.1μm, is sufficient for observation. In this case, a Shinkawa Electric type VC-020C eddy current-type sensor was used. This IMS is highly compact at 150 mm x 150 mm x 150 mm and can easily be installed in a small vacuum chamber.

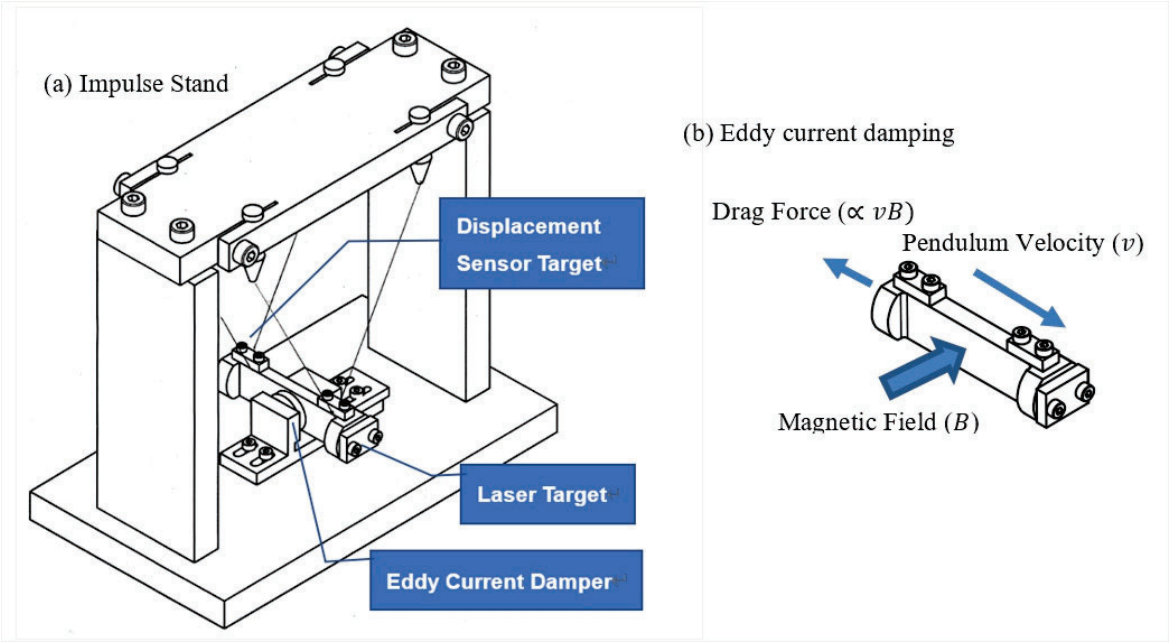

Figure 1. (a) Impulse sensor based on a simple pendulum. (b) Force generated by Eddy current. current.

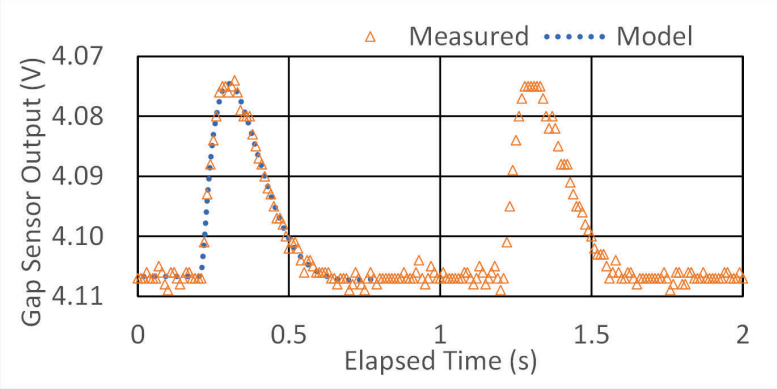

Figure 2. IMS single pulse response for 250mJ of energy.

One problem with a pendulum operating in a vacuum is damping. When the pendulum has small damping, the oscillation continues for several times its natural period, which prevents frequent measurements.[16] An effective solution to damping in a vacuum is to use eddy currents. Fig.1(b) illustrates the effect of an eddy current damping installed in the IMS. The magnetic fields are arranged to be perpendicular to the motion of the PM. The PM moves across the fields, and the eddy current generated by the motion dissipates kinetic energy and generates a drag force proportional to PM velocity and magnetic flux. The damping is adjusted by tuning the magnitude of magnetic flux. The equation of motion for the pendulum is very simple:

$$\frac{d^2x}{dt^2} + 2\gamma\frac{dx}{dt} + \omega_0^2 = 0 \tag{1}$$

where $\omega_0^2 = g/l$, g is the acceleration of gravity, and l is the effective wire length of the pendulum. The damping factor γ tuned to produce critical damping ($\gamma \sim \omega_0$) provides the fastest recovery time. Owing to the eddy current damping, the system has good linearity over three orders of magnitude, although the peak amplitude depends on γ. Fig.2 shows the tuned IMS response, with a recovery time of approximately 0.5s The system described by Eq.1 is a second-order lag system. The transfer function is

$$H(s) \propto \frac{1}{s^2 + 2s_0 s + s_0^2} \tag{2}$$

where s is the complex frequency and $s_0 = w_0/2\pi$. When a laser pulse train has a repetition frequency f_L higher than s_0, the IMS measures the average force as $F = I_m f_L$. The force F is obtained by measuring the displacement $x = Fl/Mg$. As Eq.2 can be regarded as the transfer function of the second-order low-pass filter, it is necessary to consider the filter transmission and the response delay when comparing the actual laser pulse train and the generated force.

The sensitivity of the IMS is calibrated by a simple solenoid actuator. A small permanent magnet attached to the PM generates a force proportional to the current in the coreless solenoid. When the solenoid is driven by a DC current, the generated force constant c_i is determined by the displacement of the PM according to $F = Mgx/l = c_i I_s$, where I_s represents the current. If the solenoid is driven by a pulse with a width of t_p and a current of I_s, the calibrated impulse can be found using $I_m s = Ft_p = c_i I_s$, and the response of the IMS is calibrated by this impulse. This so-called self-calibrating system is accurate linearity to 0.5% or better. Using the same calibration system, the resolution for single pulses has been confirmed to be 0.03μNs in root mean square (RMS).

2.2 Instrument Setup

The instrumentation of the impulse measurement system is shown in Fig. 3. a SPECTRA-PHYSICS GCR-230 Q-Switched Neodymium Doped Yttrium Aluminum Garnet (Q-SW Nd:YAG) laser at a wavelength of 1064nm was used. The second harmonics of the Nd:YAG laser are generated by a KD*P nonlinear crystal, which is then separated by a dichroic beam splitter. This part of the system is installed in GCR-230. The fundamental (1064nm) and SHG (532nm) beams are attenuated by the $\lambda/2$ wave plate (2) and polarizing beam splitting prism (3), respectively. Each beam is focused on the target of the impulse stand (12) by its adjustable beam expander (7). Each illuminated spot size is tuned through the focusing of the expander. The two beams of different wavelengths can be overlapped by the dichroic mirror (9). Energy meters (6) record the energy of every laser pulse, which are calibrated by the irradiated energy on the target to compensate for the loss of the optical components through the beam path. Ophir PE50BF-C and PE25BF-C are used for 1064nm and 532nm, respectively. The beam spots of 1064nm and 532nm are then redirected by the high reflection mirror (8) and the beam combiner (9), respectively. The high reflection mirror (10) controls both beams without requiring their relative positions. The spot size on the target and attenuation of the laser beam can tune the fluence on the target, which is usually measured by attenuator scanning. The various spot size data should be combined to obtain a wide range of data regarding fluence.

The IMS is placed in a vacuum chamber and maintained at a vacuum of less than 10^{-2}Pa by a turbo molecular pump and a scroll pump.

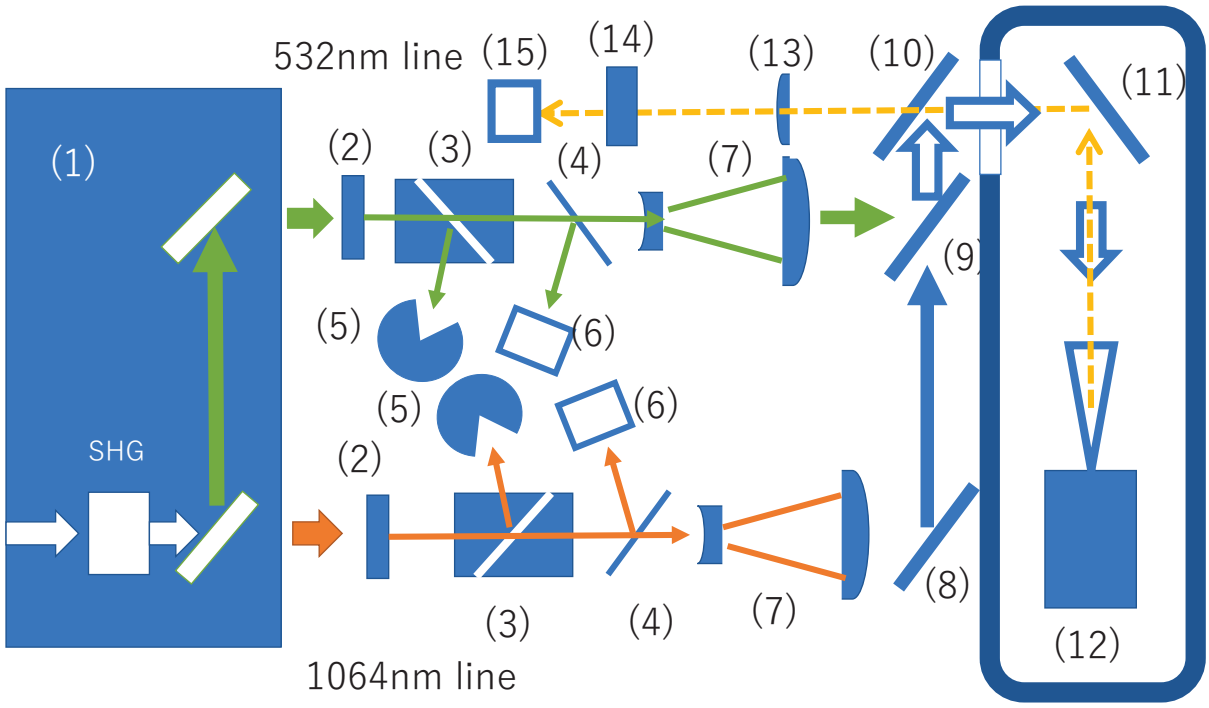

Figure 3. Diagram of the impulse measurement instruments. (1)SHG unit with beam separator as part of the GCR-230 laser, (2)$\lambda/2$ wave plate, (3)Polarizing beam splitter,(4)Beam splitter, (5)Beam damper, (6)Energy meter, (7)Beam expander and focus adjuster, (8)(10)(11)High reflection mirrors, (9)Dichroic beam combiner, (12)Impulse stand, (13) Achromatic imaging lens, (14)Filter assembly, and (15)Beam profiler

An achromatic lens (13) and beam profiler (15) monitor the spot of the irradiated laser on the target and the emission of the ablation-induced plasma with a small focus shift from visible to infrared. A filter assembly (14) has a short pass filter, 1064nm narrow band filter, 532nm narrow band filter, 532nm band rejection filter, and ND filter to observe fundamental, SHG, and ablation-induced emission separately. A combination of the 532nm band rejection and the short pass filter enables the emission to be monitored. The actual irradiated beam size is measured using the ablation mark under microscopy to obtain the laser fluence from the pulse energy. A top-hat beam profile is used to expect uniform fluence in the irradiated position. In addition, the irradiation position is defocused so large that the focal point size is on the order of 1mm. Since the defocus is large and the beam spot size of 1mm is so large that the beam waist is negligible, the beam spot shape is obtained by geometric optics and the radiated spot is obtained as a similarly reduced form of a near field profile. As a result, the near field top-hat pattern is directly transferred onto the irradiation target.[8] A comparison between the beam profile and the ablation mark confirms that ablation occurs throughout the beam, and the ablation mark is used as the most reliable beam size on the irradiation surface.

The nearly Gaussian beam profile has a smooth distribution from zero to the peak; therefore the interaction of that beam is observed as a mixture of various radiation intensities. To investigate the radiation interaction, a top-hat profile is preferable. Accordingly, the laser used in this measurement was tuned to a top hat rather than a Gaussian shape using an aperture that cuts out the central region of the profile.

The GCR-230 is designed to generate a top-hat beam profile, which is suitable for investigating the laser induced impulse and irradiating fluence and to be a good performance at the operating condition of over 10W output power for 10 to 20Hz. In the early stages of the measurement, the flash lamp was operated at a pumping frequency of 1 Hz to obtain a 1 Hz laser pulse. In that case, a profile was obtained in which the outer edge of the beam was enhanced, so a top-hat beam was obtained by removing the strong radiation in the edge using a pinhole. At the end of the measurement, the flash lamps and Q-switch are synchronously triggered at 10Hz and 1Hz, respectively, for GCR-230 laser operation, and the 1Hz laser shots with top-hat beam profile are

obtained. Since GCR-230 with 1 Hz flash lamp operation for previous work had outer edge enhanced beam profile probably caused by the improper thermal lens due to the small average heat input to Nd:YAG medium, the beam shaping aperture was used to obtain top-hat beam. The aperture has no longer necessary and is removed from the instrument setup. With this modification, the real laser energy available for measurement could be approximately doubled.

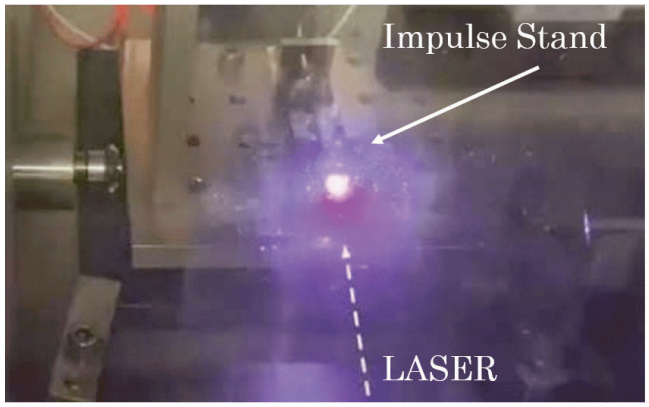

Figure 4. The impulse of the Nd:YAG Q-switched laser is measured by the impulse stand

3. MEASUREMENTS

Fig. 4 shows a jet of plasma induced by the laser during our measurement. The ablation induced hot plasma expanding in the atmosphere forms a Tayler-Sedov strong spherical shock wave, the size of the expanding sphere will not exceed about 10mm in diameter[17].[18] However, the ablation induced plasma in a vacuum freely expands in the vacuum without forming a shock wave. The jet seen in Fig. 4 is radiation from this expanding plasma, which visually extends to about 50 mm.

For 1064nm measurement, the impulses are measured with a 532nm beam path blocked or without SHG with the SHG crystal removed from the optical path. A single scan of the variable attenuator covers three to five times the fluence range. Thus, data for a given condition is usually obtained by connecting three or more data points with different spot sizes that overlap by half. The main source of system noise in the measurements is thought to be the resolution of the IMS. In the vicinity of the ablation threshold, the measurement is made with a small signal-to-noise ratio of about 10 because the laser is attenuated to irradiation energy of 20mJ or less, coupled with a small C_m. At 20 Hz, the measurement is made with a pulse width of 20ns, applying the mean power to the low-pass filter in Eq.2 improves the S/N, and C_m can be detected in the low fluence region down to 1J/cm^2. Stitched data points are seamless and smooth. The fluence can be controlled by changing the spot size without changing the profile. In addition, measurements have been made with a 1 Hz laser pulse width of 20 ns. These data agree well with an accuracy of less than ±20%, indicating that the laser energy-to-impulse conversion depends on the fluence, not the peak power of the laser.

Fig.6(A) shows the scattered image of the 1064nm irradiated image, and Fig.6(B) shows ablating plasma emission with an additional filter to reject the scattered laser. These optical images are only used for real time monitoring during the measurements. The irradiated spot size and the profile are evaluated by being measured by optical microscopy. A few of them are observed by scanning electron microscopy as shown in Fig.6(C) to verify obtaining a top-hat beam profile on the target.

Measurements at 532nm were made using a 10ns pulse, blocking the 1064nm beam. As in the case of 1064nm, the data were stitched with different beam sizes. The ablation threshold is smaller and a larger C_m is obtained compared to 1064nm.

4. DISCUSSION

In the initial measurement of ablation impulses targeting aluminum,[19] a nonlinear increase with saturation in impulse with increasing irradiation was exhibited. This effect corresponds in C_m as a linear decrease from

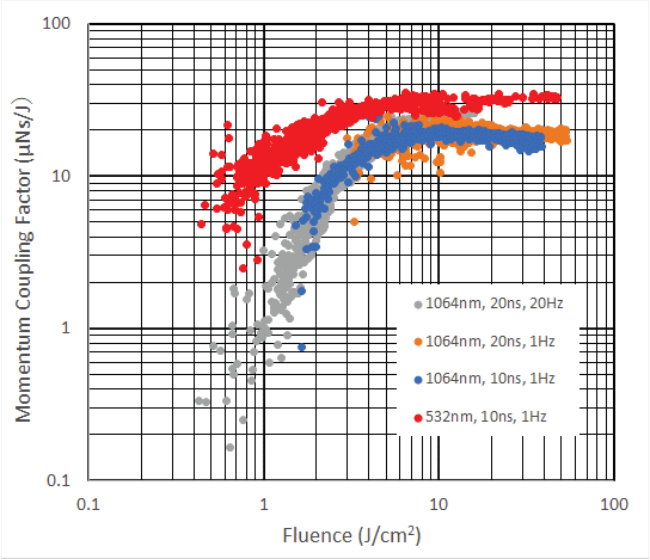

Figure 5. Measured momentum coupling factor C_m. Three cases of Nd: YAG fundamental data (1064nm) are replicated from previous work.[8] The momentum coupling factor of 532nm shows a lower threshold and higher value than that of 1064nm.

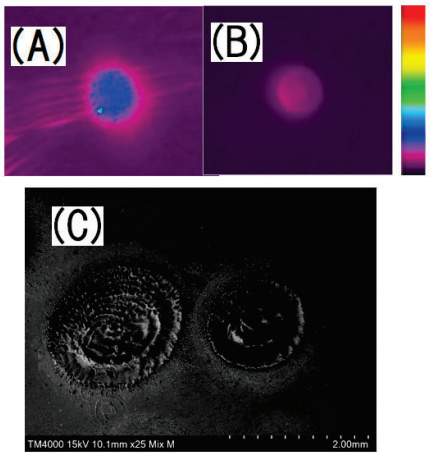

Figure 6. (A) Scattered laser image. (B) Visible emission image. (C) SEM image of the engraved crater.

20μNs/J to 15μNs/J for an increase in fluence from 5 to 15J/cm^2. This decrease in C_m is discussed as ablation suppression due to the plasma shielding effect. No attention was paid to the beam profile in this measurement, only to the beam diameter of the laser, which was measured on laser burn paper. For example, a Gaussian beam profile would contain 86% of the total beam energy in the e^{-2} diameter, but there is about an 8-fold fluence variation within the beam. In such a beam, ablation begins when the peak fluence in the beam exceeds the threshold, and only a fraction of the total beam energy contributes to ablation. As a result, impulse generation near the ablation threshold may be expected to behave in a complicated manner if the beam profile is not uniform. In the case of a laser with a non-uniform profile, the high mass removal rate in the high fluence part, the central part for above Gaussian profile, may make a deep crater. Tsuruta et al.[16] discussed the effect of the engraved craters and found the deeper crater generated less impulse. They removed the crater effects and obtained a similar result, a linear decrease from 20μNs/J to 15μNs/J for an increase from 5 to 25 J/cm^2.

To exclude such conditions in our work, the uniform profile on the irradiated surface shall be obtained using a top-hat profile laser and the aspect ratio of the crater shall be less than 0.1.

At 1064 nm, crossing the threshold, no decrease in C_m, which has been considered an effect of plasma

shielding, was observed between 5 and 50J/cm^2. At 532 nm, similarly, between 3 and 50 J/cm2, the C_m was not reduced between 3 and 50J/cm^2 at 532 nm as well.

In the case of a nanosecond laser, ablation is initiated by free electrons heating in a metal due to the electric field of laser radiation. The heat from the higher energy electrons is transferred to the crystal lattice meaning the metal melts, evaporates, and some part of which is ionized to form plasma.[20] The laser irradiation heats the plasma by inverse bremsstrahlung. Plasma formation and heating proceed simultaneously in nanosecond order. In the case of very high laser fluence, the plasma strongly absorbs the radiation so that material evaporation is suppressed. In this region, C_m decreases with a higher fluence, which is identified as the so-called plasma shielding effect.[1] The C_m plateau above approximately one order of the fluence region above a slightly higher ablation threshold, as shown in Figs. 5 , highlights how the distribution ratio of laser energy used for plasma formation and plasma heating is constant for this specific material and wavelength. In this region, so-called plasma shielding, decreasing in C_m, is not observed and ablation induced plasma characteristics, such as plasma temperature and density and so on, on the nanosecond timescale should be investigated to understand the behavior of laser induced impulse.

When the laser ablation impulse is viewed as a propulsion device, the specific impulse was obtained, giving the relationship between the consumption of the mass of the target as fuel and the total force product. The total force product and target mass loss were measured by irradiating the target with a laser pulse of approximately 5.7e6 so that the amount of target mass removal caused by laser ablation could be measured. When many laser pulses were irradiated at the same location, the crater tended to deepen and the impulse decreased. To reduce this effect, laser pulses of 400 to 600 pulses were irradiated at each of 10 irradiated points. At a fluence of 14 J/cm^2, a target mass loss of 2.9 ± 0.2mg and an integrated impulse of 44mNs are measured and a specific impulse of $(1.6 \pm 0.2) \times 10^3$s was obtained.

Ablation impulses occurring at 532 nm appear to be superior to those occurring at 1064 nm, with a lower ablation threshold and greater conversion efficiency to impulses. However, in actual systems, 532nm must be generated by SHG using a 1064nm laser, the Nd:YAG laser, which is considered the most reliable and widely used in space applications. Considering the efficiency of SHG, we cannot expect a high value of impulse generation efficiency for 1064nm laser energy. Based on the results, 20μNs/J at 1064nm and 30μNs/J at 532nm, it is better to use the 1064nm laser as it is without SHG to obtain a larger impulse, if the SHG efficiency is less than 66%,

However, SHG does not require additional power-consuming active equipment such as additional exciters or amplifiers but requires temperature-controlled nonlinear crystals, and impulses can be increased with minimal additional power. It turned out to be advantageous for space applications, which will keep the operational power at a minimum. Using SHG, not only the 532nm but also the unconverted 1064nm laser energy can be irradiated to the target and contribute to ablation, thereby improving efficiency. The impulse p generated in this case is obtained by the following Eq.3.

$$p = C_{m,532}E_{532} + C_{m,1064}E_{1064} \tag{3}$$

$$E_{total} = E_{532} + E_{1064}. \tag{4}$$

where, $C_{m,532}$, and $C_{m,1064}$ are the momentum coupling factors for 532nm and 1064nm, respectively. E_{total} is the fundamental laser energy input to the nonlinear SHG crystal, and E_{532} is SHG laser energy. E_{1064} is SHG residual energy radiated on the target. $M_{m,532,1064}$ is the nonlinear constant.

Since the configuration of a dual-wavelength simultaneous irradiation system involves issues such as wavelength aberration of the transmission optics and solving Laser Induced Damage (LID), which is a more serious problem at 532nm than at 1064nm, it is recommended to demonstrate Laser Space Debris Removal at 1064nm and promote efficiency improvement using SHG.

5. CONCLUSION

A new compact IMS has been developed for impulse measurement in a small vacuum chamber, which enables the measurement of Nd:YAG fundamental at 1064nm and SHG at 532nm.

For aluminum arroy A7075, at 1064nm, a plateau with a Momentum Coupling Factor of about 20muNs/J was observed in the range of 5J/cm^2 to 50J/cm^2, and no so-called phenomena caused by plasma shielding were observed. A specific impact of about 1600s at the fluesnce of 14J/cm^2.

At 532nm, an ablation threshold lower than that at 1064nm and a plateau of about 30muNs/J were measured.

In practical use, including SHG efficiency, 532nm component irradiation alone does not have an advantage in terms of impulse generation efficiency, but the simultaneous use of 1064nm, the residual component of SHG, indicates that a higher efficient debris removal system is possible.

ACKNOWLEDGMENTS

The authors would like to thank Mr. M. Sakashita for their support in handling and tuning the high power laser and for safety management of the laboratory area.

REFERENCES

[1] Phipps, C., Birkan, M., Bohn, W., Eckel, H.-A., Horisawa, H., Lippert, T., Michaelis, M., Rezunkov, Y., Sasoh, A., Schall, W., Scharring, S., and Sinko, J., "Review: Laser-ablation propulsion," *Journal of Propulsion and Power* **26**(4), 609–637 (2010).

[2] Wiens, R. C., Maurice, S., Barraclough, B., Saccoccio, M., Barkley, W. C., Bell, J. F., Bender, S., Bernardin, J., Blaney, D., Blank, J., Bouyé, M., Bridges, N., Bultman, N., Caïs, P., Clanton, R. C., Clark, B., Clegg, S., Cousin, A., Cremers, D., Cros, A., DeFlores, L., Delapp, D., Dingler, R., D'Uston, C., Darby Dyar, M., Elliott, T., Enemark, D., Fabre, C., Flores, M., Forni, O., Gasnault, O., Hale, T., Hays, C., Herkenhoff, K., Kan, E., Kirkland, L., Kouach, D., Landis, D., Langevin, Y., Lanza, N., LaRocca, F., Lasue, J., Latino, J., Limonadi, D., Lindensmith, C., Little, C., Mangold, N., Manhes, G., Mauchien, P., McKay, C., Miller, E., Mooney, J., Morris, R. V., Morrison, L., Nelson, T., Newsom, H., Ollila, A., Ott, M., Pares, L., Perez, R., Poitrasson, F., Provost, C., Reiter, J. W., Roberts, T., Romero, F., Sautter, V., Salazar, S., Simmonds, J. J., Stiglich, R., Storms, S., Striebig, N., Thocaven, J.-J., Trujillo, T., Ulibarri, M., Vaniman, D., Warner, N., Waterbury, R., Whitaker, R., Witt, J., and Wong-Swanson, B., "The chemcam instrument suite on the mars science laboratory (msl) rover: Body unit and combined system tests," *Space Science Reviews* **170**, 167– 227 (2012).

[3] Forshaw, J. L., Aglietti, G. S., Navarathinam, N., Kadhem, H., Salmon, T., Pisseloup, A., Joffre, E., Chabot, T., Retat, I., Axthelm, R., Barraclough, S., Ratcliffe, A., Bernal, C., Chaumette, F., Pollini, A., and Steyn, W. H., "RemoveDEBRIS: An in-orbit active debris removal demonstration mission," *Acta Astronautica* **127**, 448–463 (Oct. 2016).

[4] Yamamoto, T., Matsumoto, J., Okamoto, H., Yoshida, R., Hoshino, C., and Yamanaka, K., "Pave the way for active debris removal realization: Jaxa commercial removal of debris demonstration (crd2)," in [*Proceedings of 8th European Conference on Space Debris*], Flohrer, T., Lemmens, S., and Schmitz, F., eds., **8**, ESA, the ESA Space Debris Office, Darmstadt, Germany (May 2021).

[5] Fukushima, T., Hirata, D., Adachi, K., Itaya, Y., Yamada, J., Tsuno, K., Ogawa, T., Saito, N., Sakashita, M., Wada, S., and Ebisuzaki, T., "End-of-life deorbit service with a pulsed laser onboard a small satellite," in [*Proceedings of 8th European Conference on Space Debris*], Flohrer, T., Lemmens, S., and Schmitz, F., eds., **8**, ESA, the ESA Space Debris Office, Darmstadt, Germany (May 2021).

[6] Schall, W. O., "Orbital debris removal by laser radiation," *Acta Astronautica* **24**, 343–351 (1991). International Astronautical Federation Congress.

[7] Ebisuzaki, T., Quinn, M. N., Wada, S., Piotrowski, L. W., Takizawa, Y., Casolino, M., Bertaina, M. E., Gorodetzky, P., Parizot, E., Tajima, T., Soulard, R., and Mourou, G., "Demonstration designs for the remediation of space debris from the international space station," *Acta Astronautica* **112**, 102–113 (2015).

[8] Tsuno, K., Wada, S., Ogawa, T., Ebisuzaki, T., Fukushima, T., Hirata, D., Yamada, J., and Itaya, Y., "Impulse measurement of laser induced ablation in a vacuum," *Opt. Express* **28**, 25723–25729 (Aug 2020).

[9] Poole, H. E., Cox, J. W., Couch, R. H., and Jr., W. H. F., "A Lidar Technology Experiment From Space Shuttle: Lidar In-Space Technology Experiment (LITE)," in [*Laser Radar Technology and Applications I*], Cruickshank, J. M. and Harney, R. C., eds., **0663**, 196 – 202 (1986).

[10] Afzal, R. S., "Mars observer laser altimeter: laser transmitter," *Appl. Opt.* **33**, 3184–3188 (May 1994).

[11] Riris, H., Sun, X., Cavanaugh, J. F., Ramos-Izquierdo, L., Liiva, P., Jackson, G. B., Schmidt, S., McGarry, J., and Smith, D. E., "The lunar orbiter laser altimeter (lola) on nasa's lunar reconnaissance orbiter (lro) mission," in [*Conference on Lasers and Electro-Optics/Quantum Electronics and Laser Science Conference and Photonic Applications Systems Technologies*], *Conference on Lasers and Electro-Optics/Quantum Electronics and Laser Science Conference and Photonic Applications Systems Technologies* , CMQ1 (2008).

[12] Yu, A. W., Stephen, M. A., Li, S. X., Shaw, G. B., Seas, A., Dowdye, E., Troupaki, E., Liiva, P., Poulios, D., and Mascetti, K., "Space laser transmitter development for ICESat-2 mission," in [*Solid State Lasers XIX: Technology and Devices*], Clarkson, W. A., Hodgson, N., and Shori, R. K., eds., **7578**, 64 – 74 (2010).

[13] Hunt, W. H., Winker, D. M., Vaughan, M. A., Powell, K. A., Lucker, P. L., and Weimer, C., "Calipso lidar description and performance assessment," *Journal of Atmospheric and Oceanic Technology* **26**(7), 1214 – 1228 (2009).

[14] Straume-Lindner, A. G., "Aeolus sensor and product description," Tech. Rep. AE-SU-ESA-GS-000, ESA/ESTEC, Noordwijk, The Netherlands (Oct. 2018).

[15] do Carmo, J. P., de Villele, G., Wallace, K., Lefebvre, A., Ghose, K., Kanitz, T., Chassat, F., Corselle, B., Belhadj, T., and Bravetti, P., "Atmospheric lidar (atlid): Pre-launch testing and calibration of the european space agency instrument that will measure aerosols and thin clouds in the atmosphere," *Atmosphere* **12**(1) (2021).

[16] Tsuruta, H., Wang, B., Wang, Z., Yokota, S., and Sasoh, A., "Repetitive pulse performance of one-micrometer laser-ablation propulsion onto aluminum," *Journal of Propulsion and Power* **30**(6), 1485–1489 (2014).

[17] Porneala, C. and Willis, D. A., "Time-resolved dynamics of nanosecond laser-induced phase explosion," *Journal of Physics D: Applied Physics* **42**, 155503 (jul 2009).

[18] Yuan, H., Gornushkin, I. B., Gojani, A. B., Wang, X. H., and Rong, M. Z., "Laser-induced plasma imaging for low-pressure detection," *Opt. Express* **26**, 15962–15971 (Jun 2018).

[19] D'Souza, B. C., *DEVELOPMENT OF IMPULSE MEASUREMENT TECHNIQUES FOR THE INVESTIGATION OF TRANSIENT FORCES DUE TO LASER-INDUCED ABLATION*, PhD thesis, FACULTY OF THE GRADUATE SCHOOL,UNIVERSITY OF SOUTHERN CALIFORNIA (May 2007).

[20] Li, X. and Guan, Y., "Theoretical fundamentals of short pulse laser–metal interaction: A review," *Nanotechnology and Precision Engineering* **3**(3), 105–125 (2020).